Available online at www.sciencedirect.com
ScienceDirect
Cement and Concrete Research 38 (2008) 368–378
Cement and Concrete Research

Poromechanics analysis of a flow-through permeameter with entrapped air

George W. Scherer

Princeton University, Civil & Env. Eng./PRISM, Eng. Quad. E-319, Princeton, NJ 08544 USA

Received 18 August 2006; accepted 21 September 2007

Abstract

In a standard flow-through permeameter, a hydrostatic head is applied to one side of a sample and the flux of fluid through the sample is measured. In this paper, we apply poromechanics to calculate the evolution of the pressure distribution and the flux through the sample. We allow for negative capillary pressure in the pores at the start of the experiment (owing to self-desiccation during hydration of cement), as well as entrapped air. The time required to reach steady state flow can increase by an order of magnitude by the presence of 1 vol.% of air in the pore liquid; the delay increases as the applied pressure decreases.

Keywords: Permeability; Permeameter; Entrapped air

1. Introduction

Slow (laminar) flow of fluids through porous materials is described by Darcy's law [1], which states that the flux, J, is proportional to the gradient in pressure, p:

$$J = -\frac{k}{\eta}\nabla p \tag{1}$$

where η is the viscosity of the fluid and k is the permeability (with units of length squared). Eq. (1) is often written with the pressure replaced by the hydraulic head, h:

$$J = -k_w \nabla h = -\left(\frac{k\rho_w g}{\eta_w}\right)\nabla h \tag{2}$$

so the permeability k_w is related to k by a product of the properties of water (ρ_w=density and η_w=viscosity) and the gravitational constant, g; the conversion factor at room temperature is k_w (m/s) $\approx 10^7$ k (m^2). The most direct way to measure the permeability is to apply a pressure drop across a plate of material and to measure the flux through it. The pressure is sustained until steady state is achieved, at which point the pressure varies linearly through the sample from the applied pressure, p_A, on the inlet surface to p_O (usually atmospheric pressure) on the outlet surface. If the sample thickness is L, then the steady-state flux is

$$J_\infty = \frac{k}{\eta}\left(\frac{p_A - p_O}{L}\right) \tag{3}$$

This is simple and practical for materials of moderate to high k, such as stone and sandy soils, but can be problematic for soft materials, such as gels, or low-k materials, such as cement paste. For soft materials, the applied pressure causes significant deformation [2]. The sample must be supported on a filter or frit, and when the pressure is applied, the bottom of the sample is forced against the frit; consequently, the pore liquid is squeezed out of the compliant body, rather than being pushed through it. This results in a steep pressure gradient near the outlet side, and the rapid drainage from the sample gives the impression, if interpreted using Eq. (3), that the permeability is higher than it really is. The gradient relaxes into the linear steady state over a period of time equal to the hydrodynamic relaxation time,

$$\tau_{gel} = \frac{L^2\eta}{kH_p} \tag{4}$$

where H_p is the longitudinal modulus of the drained porous body (also known as the oedometric modulus in soil mechanics or the

E-mail address: scherer@princeton.edu.

0008-8846/$ - see front matter © 2007 Elsevier Ltd. All rights reserved.
doi:10.1016/j.cemconres.2007.09.028

stiffness c_{11}), and is related to Young's modulus, E_p, and the bulk modulus, K_p, by

$$H_p = \frac{(1-\nu_p)E_p}{(1+\nu_p)(1-2\nu_p)} = \frac{K_p}{\beta} \tag{5}$$

where ν_p is Poisson's ratio, $K_p = E_p/[3(1-2\nu_p)]$ and $\beta = (1+\nu_p)/[3(1-\nu_p)]$. Since k and H_p are both small for gels, it may take days to reach steady state. There are also difficulties in sealing a gel to the vessel, so that the experiment is difficult to reproduce [3], so less direct methods are more practical [4].

A different set of problems occurs with samples having very low permeability. For example, the permeability of cement paste is typically $<10^{-18}$ m^2, so the experiments are slow: it takes days to stabilize the flux through a sample with $k_w = 10^{-14}$ m/s [5,6]. To accelerate the flow, pressures on the order of MPa may be used, but this increases the risk of leaks or cracks that cause an overestimate of k. A thin sample can be used for homogeneous materials, but for concrete it is essential that the sample thickness be more than 3 times the diameter of the largest aggregate [7]. Much faster results can be achieved by applying a pressure pulse at the inlet [8,9] or linearly increasing the inlet pressure [10], and measuring the drop in p, rather than the flux, as liquid drains through the sample. As we shall see, however, it is particularly important to insure that the samples used in such experiments are completely saturated, because pressure relaxation is strongly affected by a small quantity of entrapped air.

In the present paper, we examine the kinetics of the approach to steady state in a flow-through permeameter, with particular attention to the case where the pore liquid contains a small amount of entrapped air. Since the air drastically increases the compressibility of the liquid, we find that 1 vol.% of air can increase the equilibration time by an order of magnitude. Further delays result if the pore liquid initially supports capillary pressure, as is often the case in cementitious materials, owing to consumption of water by the hydration process (i.e., self-desiccation leading to autogenous shrinkage [11,12]). Since the time to reach steady state is related to the permeability, the present results allow the experimentalist to check for consistency, by confirming that the measured permeability is consistent with the equilibration time. Moreover, the results show the effect of entrapped air on the kinetics of evolution of the flux, so that this problem can be detected.

In Section 2, the poromechanics analysis is presented for two boundary conditions commonly employed in flow-through permeameters: zero lateral strain (when samples are glued into a rigid cylinder) and constant confining pressure (as in a triaxial cell). The effect of air bubbles in the pore liquid is examined in Section 2.3. Calculations are presented to demonstrate the effect of capillary pressure in Section 3 and entrapped air in Section 4. The practical implications of the results are discussed in Section 5.

2. Analysis

The pressure distribution and the flux through the sample can be calculated using standard equations of poromechanics [13], based on the theory developed by Biot [14]. This approach has been applied to many problems similar to the present one, including compression of cylinders [15,16] and flow through plates [10]; it has also been used to analyze several indirect methods for measuring permeability [4]. The constitutive equations for a saturated elastic material are

$$\varepsilon_x = \frac{bp}{3K_p} + \frac{1}{E_p}\left[\sigma_x - \nu_p(\sigma_y + \sigma_z)\right] \tag{6}$$

$$\varepsilon_y = \frac{bp}{3K_p} + \frac{1}{E_p}\left[\sigma_y - \nu_p(\sigma_x + \sigma_z)\right] \tag{7}$$

$$\varepsilon_z = \frac{bp}{3K_p} + \frac{1}{E_p}\left[\sigma_z - \nu_p(\sigma_x + \sigma_y)\right] \tag{8}$$

where p is the pore pressure, ε_x, ε_y, ε_z are the strains, and σ_x, σ_y, σ_z are the total stresses. The Biot coefficient is

$$b = 1 - \frac{K_p}{K_S} \tag{9}$$

where K_S is the bulk modulus of the solid phase. The continuity equation is

$$\frac{\dot{p}}{M} + b\dot{\varepsilon} = \frac{k}{\eta}\nabla^2 p \tag{10}$$

where $\varepsilon = \varepsilon_x + \varepsilon_y + \varepsilon_z$ is the volumetric strain and the superscript dot indicates a partial derivative with respect to time. The Biot modulus, M, is defined by

$$\frac{1}{M} = \frac{\phi}{K_L} + \frac{b-\phi}{K_S} \tag{11}$$

where ϕ is the (liquid-filled) porosity and K_L is the bulk modulus of the pore liquid (or, the reciprocal of its compressibility).

In Sections 2.1 and 2.2, we will solve Eq. (10) subject to the appropriate boundary conditions. The present problem is closely related to the classical consolidation problem of soil mechanics [13, p. 125]. In Section 2.3, we will modify that equation to allow for air in the pore liquid, which drastically increases its compressibility.

2.1. Zero lateral strain

A common configuration for a flow-through permeability experiment is to seal a disk of material into a rigid ring by using epoxy or some other resin. If the sealant adheres well to the sample and the ring, then it will prevent liquid from leaking around the sample, but its effect on the deformation of the sample is difficult to predict. When the inlet pressure is applied to the surface at $z=L$, the sample will tend to contract along z and expand along x and y. If the sealant is rigid compared to the sample, or if the thickness of the layer of sealant is small and the external ring is rigid, then the lateral strain may be entirely suppressed. We will assume that this is the case in the following analysis. If the sample adheres well to the sealant and the sealant

is rigid, then the vertical strain (ε_z) will also be suppressed at the boundary; however, ε_z will increase toward the center of the disk. We will assume that the width of the disk is large enough so that most of the area is not affected by the vertical constraint at the boundary. If the sample is rigid compared to the sealant (as would be the case for concrete sealed by epoxy), then the sealant will deform and the sample will contract uniformly along z. If the sample is not wide and the sealant is stiff, then the strain will be suppressed in all directions; that case would be described by setting the parameter Λ equal to 0 in the following equations. Finally, we must assume that the sample is supported on a rigid porous frame on the outlet side, so that the disk does not bend.

If the sample cannot expand laterally when pressure is applied on the inlet face, then we can assume that $\sigma_x=\sigma_y$ and $\varepsilon_x=\varepsilon_y=0$. In this case, Eq. (6) becomes

$$\frac{bp}{3K_p}+\frac{1}{E_p}\left[\sigma_x\left(1-\nu_p\right)-\nu_p\sigma_z\right]=0 \tag{12}$$

which can be solved for σ_x in terms of σ_z. If the applied pressure on the inlet face ($z=L$) is p_A, then $\sigma_z=-p_A$. With these conditions, Eqs. (8) and (12) lead to

$$\varepsilon_z=\varepsilon=\frac{bp-p_A}{H_p} \tag{13}$$

Using Eq. (13), and recognizing that flow occurs exclusively along the z direction (because the edges of the sample are sealed), the continuity equation becomes

$$\frac{\partial p}{\partial\theta}-\Lambda\frac{\partial p_A}{\partial\theta}=\frac{\partial^2 p}{\partial u^2} \tag{14}$$

where $u=z/L$, L is the thickness of the sample, the reduced time is $\theta=t/\tau_v$ and the hydrodynamic relaxation time is

$$\tau_v=\left(\frac{\eta L^2}{k}\right)\left(\frac{b^2}{H_p}+\frac{1}{M}\right)=\left(\frac{\eta L^2}{kH_p}\right)\left(\frac{b}{\Lambda}\right) \tag{15}$$

Finally, the constant Λ is defined as

$$\Lambda=\frac{b}{b^2+H_p/M} \tag{16}$$

In the "gel limit", where $K_p<<K_L$ or K_S, the second term in the denominator of Eq. (16) is negligible and $b\approx 1$, so $\Lambda\approx 1$ and τ_v becomes equal to τ_{gel} defined in Eq. (4). An estimate of the porosity range where the gel limit applies can be found from the bound given in ref. [13], Eq. (4.37a):

$$\frac{K_p}{K_S}\le\frac{1-\phi}{1+\frac{(1+\nu_S)\phi}{2(1-2\nu_S)}} \tag{17}$$

where ν_S is the Poisson's ratio of the solid phase. This leads to

$$b\ge\frac{\phi}{1-\beta_S+\beta_S\phi}\xrightarrow{\nu_S=0.2}\frac{2\phi}{1+\phi} \tag{18}$$

where $\beta_s=(1+\nu_s)/[3(1-\nu_s)]$. Thus, for $\nu_S\approx 0.2$, given the typical porosity of gels ($\phi>0.95$), Eq. (18) gives $b>0.97$, so it is reasonable to approximate b as unity.

For more rigid materials, where $K_L<<K_p$ or K_S, then the Biot modulus reduces to $M\approx K_L/\phi$ and Eq. (16) reduces to

$$\Lambda\approx\frac{\beta bK_L}{\phi K_p} \tag{19}$$

The relaxation time becomes

$$\tau_v\approx\left(\frac{\eta L^2}{k}\right)\left(\frac{\phi}{K_L}\right) \tag{20}$$

Thus, the rate of relaxation of the pore pressure is controlled by the softer phase (*viz*., the solid network in a gel and the liquid in a rock or cement paste).

The boundary conditions are that the pressure applied on the inlet face is $p_A(\theta)$, while the constant pressure p_O (usually atmospheric pressure) is sustained on the outlet face. The interior of the sample is initially p_i, which is assumed to be either equal to p_O or to represent capillary pressure related to the internal relative humidity (RH), according to

$$p_i=p_O+\frac{R_gT}{V_L}\ln(\mathrm{RH}) \tag{21}$$

where R_g is the ideal gas constant, T is absolute temperature, and V_L is the molar volume of the liquid. A substantial negative capillary pressure can arise in cement paste without draining a significant fraction of the pores, owing to the small size of the breakthrough radius into the percolating pore network. This is particularly true for high-performance (low w/c) materials, as can be seen from the shallow slope of the desorption curve for RH ≥ 0.85 in Fig. 4 of ref. [17].

The solution of Eq. (14) subject to these conditions is discussed in Appendix A. The pore pressure is found to be

$$p(u,\theta)=p_i+(p_O-p_i)\Omega_0(u,\theta)+\int_0^\theta\left[\Omega_1(u,\theta-\theta')+\Lambda\Omega_2(u,\theta-\theta')\right]\frac{\partial p_A}{\partial\theta'}d\theta' \tag{22}$$

where the relaxation functions are

$$\Omega_0(u,\theta)=1-u+\sum_{n=1}^{\infty}\frac{2(-1)^n\sin[n\pi(1-u)]}{n\pi}\exp\left(-n^2\pi^2\theta\right) \tag{23}$$

$$\Omega_1(u,\theta)=u+\sum_{n=1}^{\infty}\frac{2(-1)^n\sin[n\pi u]}{n\pi}\exp\left(-n^2\pi^2\theta\right) \tag{24}$$

$$\Omega_2(u,\theta)=\sum_{n=1}^{\infty}\frac{2[1-(-1)^n]\sin[n\pi u]}{n\pi}\exp\left(-n^2\pi^2\theta\right) \tag{25}$$

When $\theta=0$, $\Omega_0=\Omega_1=0$ and $\Omega_2=1$; as $\theta\to\infty$, $\Omega_0\to 1-u$, $\Omega_1\to u$, and $\Omega_2\to 0$. These functions are illustrated in Fig. 1.

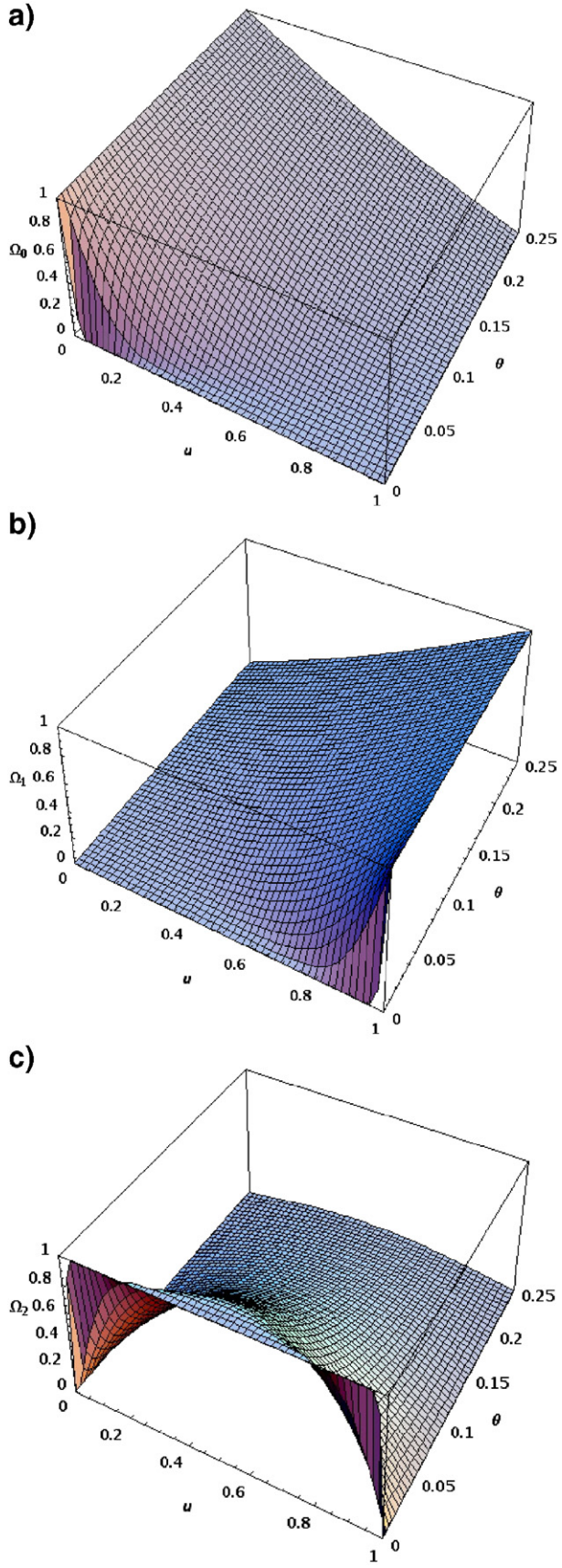

Fig. 1. Relaxation functions defined in Eqs. (23) (24) (25) .

If p_A makes a step change at $\theta=0$ and then remains constant, the solution reduces to

$$p(u,\theta) = p_i + (p_O - p_i)\Omega_0(u,\theta) + (p_A - p_i)[\Omega_1(u,\theta) + \Lambda\Omega_2(u,\theta)] \quad (26)$$

At the moment the pressure is applied to the inlet face, the pore pressure is

$$p(u,0) = p_i + \Lambda(p_A - p_i) \quad (27)$$

In the gel limit ($\Lambda \approx 1$), this means that the pore pressure throughout the sample jumps to the applied pressure at $\theta=0$. The liquid then drains from the outlet face until a linear pressure drop develops [2]:

$$p(u,\theta\rightarrow\infty) = p_O + (p_A - p_O)u \quad (28)$$

In the following, we will consider only the case where the inlet pressure is constant. The flux through the sample is found by taking the derivative of Eq. (26):

$$\left.\frac{\partial p}{\partial u}\right|_{u=0} = (p_A - p_O) + 2\sum_{n=1}^{\infty}\{(p_A - p_i)[\Lambda + (1-\Lambda)(-1)^n] - (p_O - p_i)\}\exp\left(-n^2\pi^2\theta\right) \quad (29)$$

The flux from the outlet surface, normalized by the steady-state flux from Eq. (3), is

$$\frac{J(0,\theta)}{J_\infty} = 1 + 2\sum_{n=1}^{\infty}\left\{\left(\frac{p_A - p_i}{p_A - p_O}\right)[\Lambda + (1-\Lambda)(-1)^n] - \left(\frac{p_O - p_i}{p_A - p_O}\right)\right\}\exp\left(-n^2\pi^2\theta\right) \quad (30)$$

If $p_i=p_O$ (i.e., if the internal RH=1), this reduces to

$$\frac{J(0,\theta)}{J_\infty} = 1 + 2\sum_{n=1}^{\infty}[\Lambda + (1-\Lambda)(-1)^n]\exp\left(-n^2\pi^2\theta\right) \quad (31)$$

As shown in Appendix A, at early times the flux is given approximately by

$$\frac{J(0,\theta)}{J_\infty} \approx \left[\Lambda\left(\frac{p_A - p_i}{p_A - p_O}\right) - \left(\frac{p_O - p_i}{p_A - p_O}\right)\right]\frac{1}{\sqrt{\pi\theta}} \quad (32)$$

For gels, $\Lambda \approx 1$, so when $p_i=p_O$ the initial flux is $J \sim J_\infty/(\pi\ \theta)^{1/2}$, which means that it decreases toward its equilibrium value. For more rigid materials, Λ is small, so the flux is initially low and rises toward equilibrium. We will see in Section 3 that materials of intermediate stiffness exhibit a minimum in $J(0,\theta)$ (see Fig. 4).

If the internal RH<1, then the capillary pressure will draw liquid into both faces (assuming that the outlet face is in contact with liquid, as is often the case). The condition for influx into the outlet face is found by making the flux negative in Eq. (32):

$$\Lambda\left(\frac{p_A+|p_i|}{p_A-p_O}\right)-\left(\frac{p_O+|p_i|}{p_A-p_O}\right)<0 \tag{33}$$

As long as $p_A>p_O$, this reduces to

$$|p_i|>\frac{\Lambda p_A-p_O}{1-\Lambda} \tag{34}$$

This condition can also be derived from Eq. (27) by recognizing that influx occurs when the internal pressure is lower than p_O.

2.2. Constant confining pressure

Permeability is often measured in a triaxial cell where the sample is surrounded by a flexible tube that is pushed against the sample by pressurized fluid. The confinement pressure, p_C, must be sufficient to suppress leaks around the sample. It is obvious that leakage from the sample will occur unless $p_C>p_A$, but experience indicates that p_C should exceed 4 p_A [6]. In this case, the boundary conditions are $\varepsilon_x=\varepsilon_y$ and $\sigma_x=\sigma_y=-p_C$, so

$$\varepsilon_x=\varepsilon_y=\frac{bp}{3K_p}+\frac{1}{E_p}\left[-p_C(1-\nu_p)+\nu_p p_A\right] \tag{35}$$

From this we see that the lateral strain is not constant through the thickness of the sample, owing to the variation of p with z. This complicates the analysis, because shear strains must be present if $\varepsilon_x=\varepsilon_x(z)$. We can avoid this issue by assuming that the confining pressure is somehow applied through a rigid surface, so that the lateral strain is uniform, but that is artificial and it leads to an implicit solution for the pore pressure. Since the results are quite similar to the case of zero strain, we will not present the results. We simply comment on some of the features of the experiment.

The average lateral strain of the sample is found from Eq. (35):

$$\int_0^1 \varepsilon_x du=\frac{\langle p\rangle b}{3K_p}+\frac{1}{E_p}\left[-(1-\nu_p)p_C+\nu_p p_A\right] \tag{36}$$

where $\langle p\rangle$ is the average pressure, defined by

$$\langle p\rangle=\frac{1}{L}\int_0^L p(z,\theta)dz=\int_0^1 p(u,\theta)du \tag{37}$$

At steady state, $\langle p\rangle=p_A/2$, so Eq. (36) indicates that the average lateral strain is zero if the confining pressure is

$$p_C=\frac{\left[(1-2\nu_p)b+2\nu_p\right]p_A}{2(1-\nu_p)} \tag{38}$$

For cementitious materials, where $\nu_p=0.2$ [18] and $b\approx 0.6$ [19], this reduces to $p_C\approx p_A/2$, which is too small to prevent leaks [6]. Thus, the confinement pressure must be sufficient to cause a net lateral compression of the sample. This could close small cracks in the sample and reduce the permeability, compared to what would be measured in a permeameter where the sample is glued into place with lateral stress given by Eq. (38).

If the confining pressure is applied before the driving pressure, then the sample will be compressed laterally and liquid will begin to drain symmetrically to its upper and lower faces. The time required for the pore pressure to equilibrate will be on the order of $\tau_\nu/3$. If the confining pressure and the driving pressure are applied simultaneously, then the equilibration time will still be on the order of $\tau_\nu/3$, but the initial flux will include contributions from the lateral compression. Since p_C must be greater than p_A, there will be an outward flux at the upper surface before the driving pressure reverses the flow. Fig. 2 shows the rate of relaxation of the pore pressure at the midplane, $(p(1/2,\theta)-p_0)/(p_C-p_0)$, which is proportional to $\Omega_2(1/2,\theta)$.

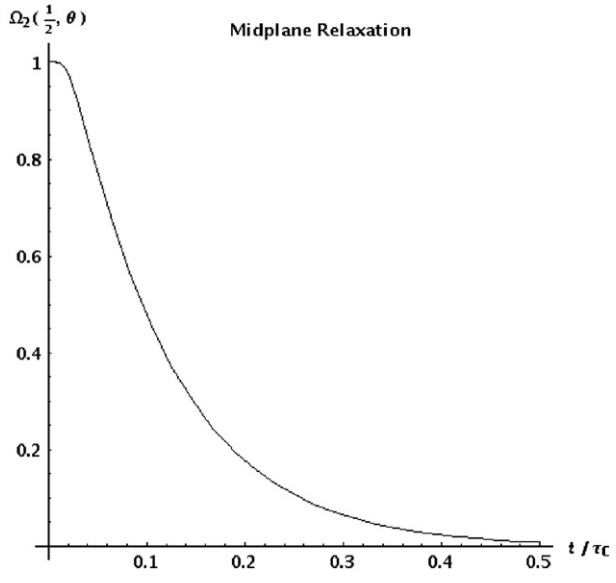

Fig. 2. Relaxation function at the midplane ($u=1/2$) of the plate. This curve represents the kinetics of relaxation of the pore pressure created at the center of the plate when lateral confinement is imposed.

2.3. Entrained air

In many porous materials, but particularly in cementitious materials with a low water/cement ratio, it is difficult to achieve perfect saturation of the sample. This is important in a permeability measurement, because a small amount of air bubbles drastically increases the compressibility of the pore liquid. If many small bubbles are uniformly distributed throughout the pore liquid, then the system of liquid and gas can be treated as a homogeneous composite. We assume that the size of these bubbles is at least on the micron scale, so that the capillary pressure within them is close to atmospheric. If the bubbles were in the mesopores with nanometric radii, their internal pressure would be so high that their compressibility

would be small (as explained below) and they would not have much influence on the experiment.

As suggested in ref. [20], the apparent bulk modulus, K_L^A, of a liquid containing a volume fraction v of bubbles of an ideal gas can be approximated as

$$\frac{1}{K_L^A} = \frac{1-v}{K_L} + \frac{vp_0}{p^2} \tag{39}$$

We assume that the bubbles were initially entrained with an internal pressure of p_O and $v = v(p_0)$. As the pressure increases, the volume fraction of bubbles decreases to $v\ p_0/p$; the compressibility of an ideal gas is $1/p$, so the last term in Eq. (39) represents the current volume fraction of air times its compressibility. The coefficient of $1/K_L$ is approximate, because it does not account for the pressure dependence of v, but the error is small, because we are only interested in low air contents where $1-v \approx 1$.

Suppose that the pore liquid is water, so $K_L = 2.2$ GPa [21], and that the applied pressure is $p_A = 10$ atmospheres, so near the inlet surface $p = 10$ $p_O = 1$ MPa. Then, Eq. (39) indicates that 1 vol.% air ($v = 0.01$) reduces the bulk modulus of the pore liquid to $K_L^A = 0.69$ GPa; at the lower surface of the sample, where $p \approx p_O$, $K_L^A \approx 0.01$ GPa. The rate of relaxation of the pore pressure is inversely related to the bulk modulus of the liquid, according to Eq. (20), so a small amount of air will profoundly affect the time to reach steady state. Note that if the air were in pores with radii of 140 nm, the capillary pressure in the bubbles would be 1 MPa, so the impact of the air on K_L^A would be drastically reduced.

Unfortunately, use of Eq. (39) introduces a nonlinear term into the continuity equation, which becomes[1] [20]

$$\frac{\dot{p}}{M_v} + b\dot{\varepsilon} + \frac{\phi v p_0 \dot{p}}{p^2} = \frac{k}{\eta}\nabla^2 p \tag{40}$$

where we redefine the Biot modulus as

$$\frac{1}{M_v} = \frac{\phi(1-v)}{K_L} + \frac{b-\phi}{K_S} \tag{41}$$

When the lateral strain is zero, Eq. (40) becomes

$$\frac{\partial p}{\partial \theta}\left(1 + \frac{c}{p^2}\right) - \Lambda \frac{\partial p_A}{\partial \theta} = \frac{\partial^2 p}{\partial u^2} \tag{42}$$

where

$$c = \frac{\Lambda H_p v \phi p_O}{b} \tag{43}$$

Eq. (42) must be solved numerically. The solution was obtained using the function NDSolve in Mathematica® [22], as explained in Appendix B.

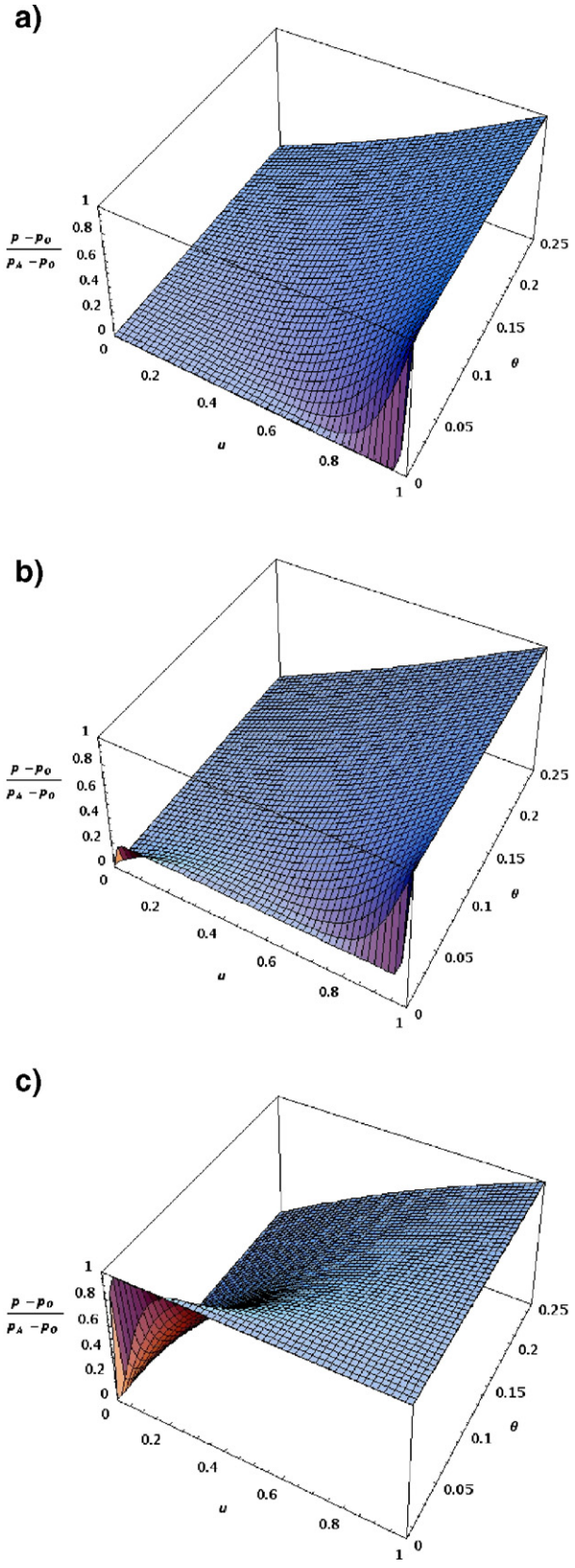

Fig. 3. Pressure in sample in which the initial pore pressure is atmospheric ($p_i = p_O$). a) Perfectly rigid ($\Lambda = 0$); b) Typical cement paste ($\Lambda = 0.21$); c) Gel limit ($\Lambda = 1$).

[1] Olivier Coussy (private communication) has shown that there is an additional term on the right side of Eq. (40) that is proportional to $(\nabla p)^2$. However, for the range of property values used here, and for air contents as high as 10%, numerical evaluations shows that term to be negligible, so it is not included in the calculations presented below.

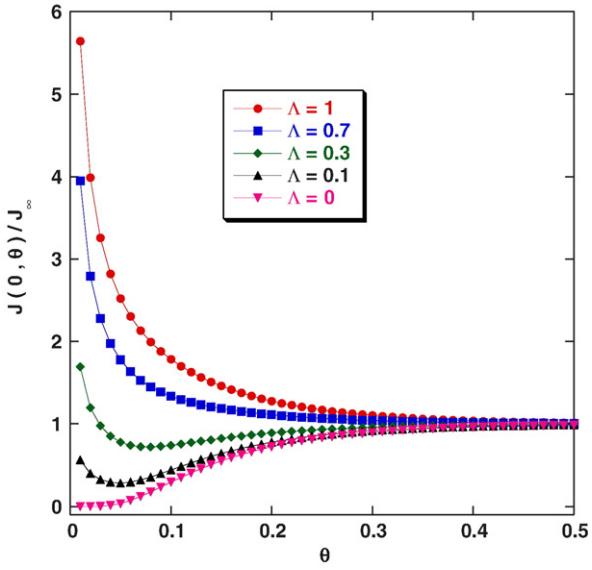

Fig. 4. Normalized flux when $p_i=p_O$ calculated using Eq. (31).

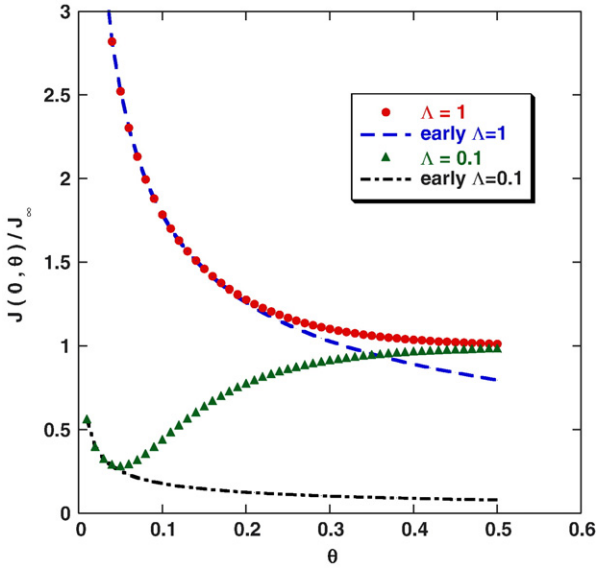

Fig. 5. Normalized flux from Eq. (31) compared to approximation given by Eq. (32).

All of the following calculations are for the case of zero lateral strain, where the inlet pressure increases instantly to $p_A=1$ MPa at $t=0$ and then remains constant. In several of the following illustrations, we arbitrarily choose $\Lambda=0.21$, which corresponds to the properties of a cement paste with $w/c=0.6$ used in a previous study ($\nu_p=0.2$, $K_p=6.3$ GPa, $\phi=0.53$, $b=0.73$) [19,23].

3. Saturated samples

3.1. No capillary pressure ($p_i=p_O$)

In this case, the pressure distribution through the sample is given by Eq. (26) with $p_i=p_O$:

$$\frac{p(u,\theta)-p_O}{p_A-p_O}=\Omega_1(u,\theta)+\Lambda\Omega_2(u,\theta) \tag{44}$$

Since $\Omega_1(u,0)=0$ and $\Omega_2(u,0)=1$, the right side of Eq. (44) equals Λ when $\theta=0$. This is shown in Fig. 3 for several values of Λ. In the gel limit (Fig. 3c, $\Lambda=1$), the pore pressure immediately jumps up to p_A, then begins to drop near the outlet side as liquid drains from the pores; by the time that $\theta\approx0.25$, a linear pressure drop has developed. In the perfectly rigid case (Fig. 3a, $\Lambda=0$), there is no deformation of the porous solid by the pressure, so the pore pressure remains at p_O when θ is small; the pressure gradient continuously increases with time until the linear profile appears. For intermediate cases (e.g., Fig. 3b), the pressure jumps to a value related to Λ, then drops near the outlet and rises near the inlet until the steady-state profile is achieved.

The dependence of the flux on Λ is shown in Fig. 4. For all compressible samples ($\Lambda>0$), the initial flux is high, because liquid is squeezed from the pores near the outlet surface. In the gel limit, the flux decreases continuously, but for lower values of Λ (characteristic, for example, of cement paste) the flux passes through a minimum before rising to steady state. The performance of the early-time approximation in Eq. (32) is illustrated in Fig. 5. All of the curves reach steady state at about the same reduced time ($\theta\approx0.3$), but this corresponds to different actual times, since the relaxation time decreases as the rigidity of the porous body increases (for fixed k and L).

3.2. Effect of capillary pressure

Cementitious bodies can develop high internal capillary pressure owing to consumption of water by the hydration reaction, resulting in internal relative humidities as low as 60–70% [12]. The corresponding suction calculated from Eq. (21) is enormous, as shown in Fig. 6. When $p_i<p_O$, liquid will flow

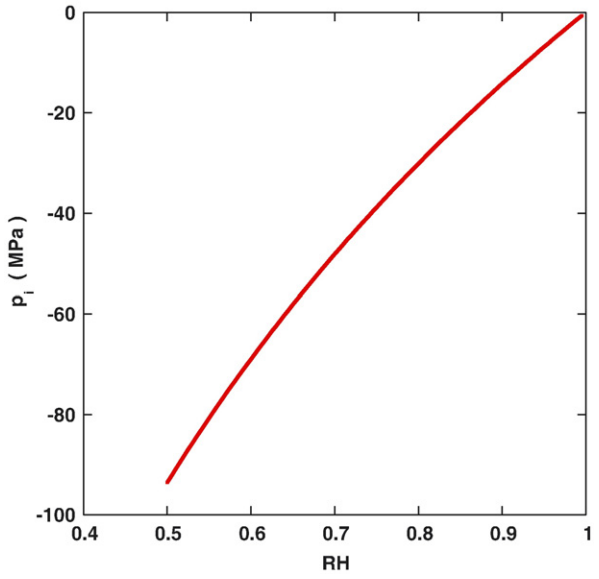

Fig. 6. Capillary pressure of water, calculated from Eq. (21), using $V_L=18$ cm^3/mol, $T=293$ K, and $R_g=8.3$ J/mol K.

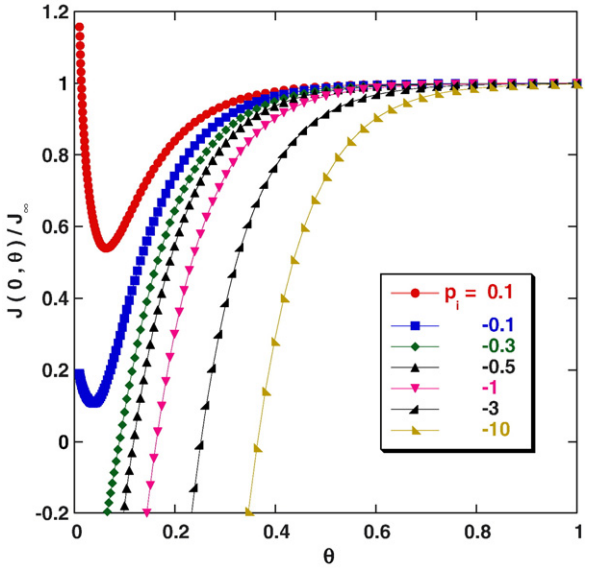

Fig. 7. Normalized flux calculated using Eq. (30) for various initial capillary pressures, p_i, assuming $\Lambda=0.21$.

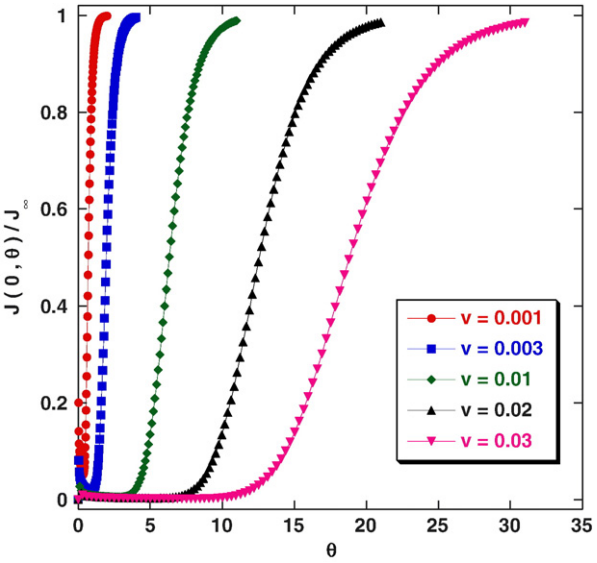

Fig. 9. Normalized flux in sample with $p_i=p_O=0.1$ MPa, $\Lambda=0.21$, containing various volume fractions, v, of air.

into the outlet face, if it is in contact with liquid (as is commonly the case). As indicated in Fig. 7, the time to reach steady state is significantly extended when capillary pressure is initially present; for example, when $p_i=-10$ MPa (RH $\approx$ 0.93) the delay is roughly tripled. In these calculations it is assumed that the air content in the pore liquid is zero, which means that the menisci are on the external surface of the sample.

4. Effect of entrained air

The most dramatic changes in kinetics occur when entrapped air is present in the material. Fig. 8 shows the pressure distribution within a sample containing 1 vol.% air ($p_i=p_O=0.1$ MPa). The air raises the compressibility of the pore liquid so much that the pressure remains at p_O when p_A is applied. The steady state gradient is not achieved until $\theta>10$, which is ~35 times longer than when $v=0$, as can be seen by comparison with Fig. 4. Fig. 9 illustrates the profound influence of air content on the time to approach steady state when $p_A=1$ MPa.

As the inlet pressure increases, the rate of flow into the sample rises, so the bubbles are more quickly compressed and steady state is achieved in a time that is roughly inversely proportional to p_A. If the outlet pressure is also elevated, then the bubbles will be compressed (and consequently "stiffer") at the outset. These points are illustrated in Fig. 10. When

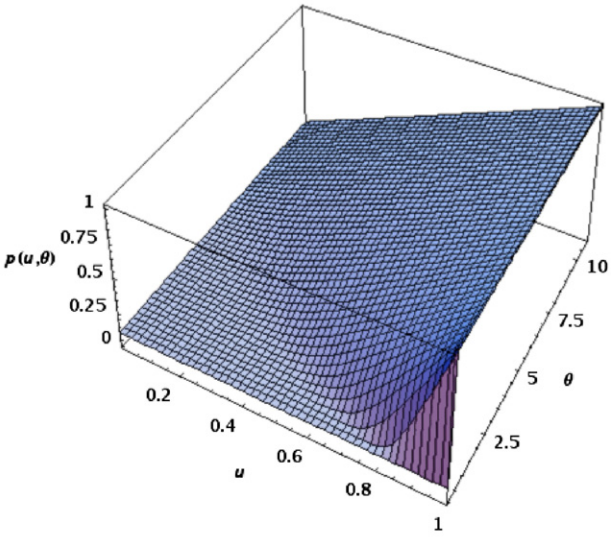

Fig. 8. Pressure distribution in a sample with $p_i=p_O=0.1$ MPa, and an air content of $v=0.01$.

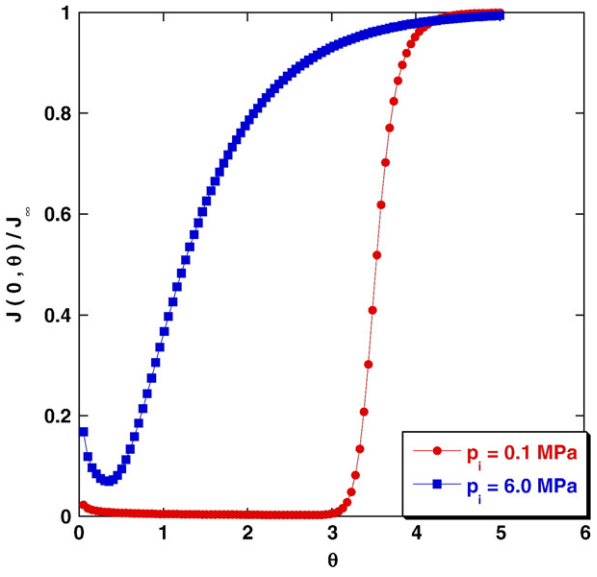

Fig. 10. Flux from sample containing 3 vol.% air ($v=0.03$), subjected to inlet pressure $p_A=7$ MPa, with initial pore pressure of $p_i=p_O=0.1$ or 6.0 MPa.

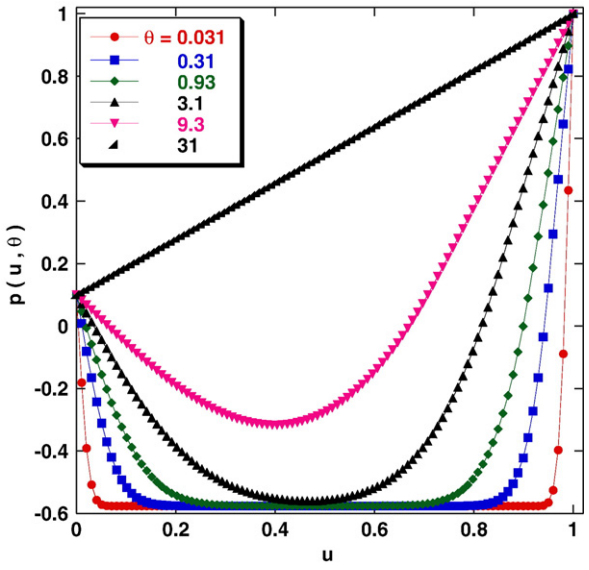

Fig. 11. Pressure distribution within a sample whose internal RH=0.995, so p_i=−0.57 MPa; the inlet pressure is p_A=1.0 MPa and the outlet pressure is p_O=0.1 MPa.

p_i=p_O=0.1 MPa, there is no flux at the moment that the inlet pressure is raised to p_A=7 MPa, but the faster flux produced by that pressure leads to a steady state in about 1/7 the time required when p_A=1 MPa (see Fig. 9). When p_i=p_O=6 MPa, Eq. (39) indicates that the pore liquid is less compressible, so the initial pressure causes a sudden flux, similar to the behavior of samples without air bubbles. However, the time to reach steady state is not strongly dependent on the outlet pressure.

The equilibration time is lengthened when capillary pressure is present, but the effect is relatively small. Consider the case where the internal RH is reduced to 0.995, so that p_i=−0.58 MPa, and v=0.01. At this RH, relatively little pore emptying will occur, so the bubbles initially present will not have grown much, and their internal pressure will be close to p_O=0.1 MPa. The evolution of the pressure profile following application of p_A=1 MPa is shown in Fig. 11. Clearly, the delay caused by the capillary pressure is negligible compared to the effect of the air. If the initial RH were much lower, then substantial pore emptying would occur; the rate of approach to steady state would then be long, but it would be more affected by the additional air-filled pores than by the reduced pressure in the liquid.

5. Discussion and conclusions

When the permeability is calculated from the steady state equation, Eq. (3), the experimenter should confirm that the time elapsed before measurement was at least $\tau_v/3$, where the relaxation time is given by Eq. (15). The time to reach steady state will be much longer than that if there is significant capillary pressure in the pore liquid, but if that is so, it will be revealed by flow into the outlet face at the start of the experiment.

The most dramatic effect on equilibration time results from entrapped air. As indicated in the simulations, just 1 vol.% air in the pore liquid can increase the time to reach steady state by as much as two orders of magnitude. Therefore, the sample should be saturated with care, and the pore liquid should be de-aired before use. Fortunately, although the presence of air causes delay, it does not change the outcome of the experiment. The calculations show that the final flux is still given by Eq. (3). Moreover, the shape of the curve of flux versus time is altered: rather than having an initial decrease in the flux according to Eq. (32), the flux rises continuously. It is advisable, therefore, to follow the flux from the moment that the inlet pressure is applied, so that the presence of air can be detected.

It is interesting to contrast the effect of entrapped air on the flow-through permeameter and the dynamic pressurization (DP) permeameter [20,23]. In the DP method, a sample is submerged in liquid and subjected to a hydrostatic pressure, which causes an initial compression; as the surrounding liquid flows into the pores and raises the internal pressure, the sample re-expands. By measuring the kinetics of dilatation, the permeability can be calculated. Using the same method of calculation as in Section 2.3, it was shown that, under a hydrostatic pressure of 7 MPa, 1% air could retard equilibration by about a factor of ~2. This is far smaller than the order of magnitude delay shown in Fig. 10 for the flow-through permeameter, where much of the pore liquid is subject to low pressure, so it remains highly compressible. Moreover, in the DP experiment, the permeability is found from the data during the period of equilibration, whereas the measurement of the flux in the flow-through permeameter only begins after that time, and may have to continue for quite a while when the flux is small.

The pressure decay method of Brace et al. [8] is subject to very serious errors if entrapped air is present, because the pressure pulse will be relaxed by compression of the bubbles, rather than flow through the sample. This would be reflected in a reduction of pressure on the inlet side that is incommensurate with the pressure increase on the outlet side; therefore, it is essential to measure both pressures when using that technique.

Even in the absence of air, dynamic pressurization [20] and pressure decay [8] are much faster than the flow-through method. If the sample is uncracked, then the DP method is advantageous, because it is fast and is not subject to errors from leaks. On the other hand, if the objective is to evaluate the effect on permeability of cracks that penetrate the sample, then only the flow-through method is satisfactory. If the material is homogeneous enough to be formed into a slender beam, and if the permeability is low (say, $k<10^{-18}$ m^2), then the beam-bending method [4,19,24,25] is ideal, because it is fast and additionally provides the elastic (and even viscoelastic) properties of the body. If it is not possible to prepare a sample of such a material in that shape, then the permeability can be extracted from the thermal expansion kinetics [4,26,27], and the measurement can be done using a conventional differential mechanical analyzer [28].

Acknowledgments

The author is indebted to Doug Hooton (University Of Toronto) for helpful discussions regarding permeability measurements and

to Olivier Coussy (Institut Navier) for thoughtful comments on the analysis.

Appendix A. Solution of Eq. (14)

The initial pore pressure is p_i, so taking the Laplace transform [29] with respect to θ,

$$L\left[\frac{\partial p}{\partial \theta}\right] = s\,\hat{p} - p_i \tag{45}$$

where s is the transform parameter and the circonflex indicates a transformed function. Similarly, the pressure on the inlet surface must jump from p_i to p_A, so

$$L\left[\frac{\partial p_A}{\partial \theta}\right] = s\,\hat{p}_A - p_i \tag{46}$$

The transform of the continuity equation is therefore

$$\frac{\partial^2 \hat{p}}{\partial u^2} - s\,\hat{p} = -(1-\Lambda)p_i - \Lambda s\,\hat{p}_A \tag{47}$$

The boundary condition on the inlet surface is

$$\hat{p}(1,s) = \hat{p}_A \tag{48}$$

and on the outlet surface, where a constant pressure p_O is applied,

$$\hat{p}(0,s) = p_O/s \tag{49}$$

The solution of Eq. (47), subject to conditions (48) and (49), is

$$\hat{p}(u,s) = \frac{p_i}{s} - (p_O - p_i)\left[\frac{1}{s} - \hat{\Omega}_0(u,s)\right] + (s\,\hat{p}_A - p_i)\left[\hat{\Omega}_1(u,s) + \Lambda\hat{\Omega}_2(u,s)\right] \tag{50}$$

where the transformed relaxation functions are

$$\hat{\Omega}_0(u,s) = \frac{\sinh[(1-u)\sqrt{s}]}{s\sinh[\sqrt{s}]} \tag{51}$$

$$\hat{\Omega}_1(u,s) = \frac{\sinh[u\sqrt{s}]}{s\sinh[\sqrt{s}]} \tag{52}$$

$$\hat{\Omega}_2(u,s) = 1 - \hat{\Omega}_0(u,s) - \hat{\Omega}_1(u,s) \tag{53}$$

Appendix B. NumericRal solution of Eq. (42)

The numerical solution of the continuity equation for a body whose pores contain gas pockets in the liquid, Eq. (42), was obtained using the function NDSolve in Mathematica® [22]. The routine cannot accept boundary or initial conditions at zero, so the initial conditions were specified at $\theta = 10^{-10}$ and the boundary conditions were applied at $u = 10^{-10}$. To avoid a discontinuity in the boundary condition, the pressure jump was written as

$$p(1,\theta) = p_0 + (p_A - p_0)\tanh\left(10^4\theta\right) \tag{54}$$

The maximum step size for u and θ was set to 10^{-3}, which was sufficient to eliminate messages indicating failure to converge. When the volume fraction of air was set to a value $\leq 10^{-3}$, the numerical solution converged on the analytical solution for the air-free case. The solution for $p(u,\theta)$ is returned as an interpolating function, which can be used to plot or list the pressure, or differentiated to get the flux. The pressure distributions in Figs. 3 and 8 were produced from the interpolating function using the Mathematica® plotting function, Plot3D.

References

[1] J. Happel, H. Brenner, Low Reynolds number hydrodynamics, Martinus Nijhoff, Dordrecht, 1986.
[2] G.W. Scherer, Measurement of permeability: I. Theory, J. Non-Cryst. Solids 113 (2-3) (1990) 107–118.
[3] G.W. Scherer, R.M. Swiatek, Measurement of permeability: II. Silica Gel, J. Non-Cryst. Solids 113 (2–3) (1990) 119–129.
[4] G.W. Scherer, Characterization of saturated porous bodies, Concr. Sci. Eng. 37 (265) (2004) 21–30.
[5] A.S. El-Dieb, R.D. Hooton, Water-permeability measurement of high performance concrete using a high-pressure triaxial cell, Cem. Concr. Res. 25 (6) (1995) 1199–1208.
[6] A.S. El-Dieb, R.D. Hooton, A high pressure triaxial cell with improved measurement sensitivity for saturated water permeability of high performance concrete, Cem. Concr. Res. 24 (5) (1994) 854–862.
[7] R.D. Hooton, What is needed in a permeability test for evaluation of concrete quality? in: L.R. Roberts, J.P. Skalny (Eds.), Pore Structure and Permeability of Cementitious Materials, vol. 137, Materials Research Society, Pittsburgh, PA, 1989, pp. 141–149.
[8] W.F. Brace, J.B. Walsh, W.T. Frangos, Permeability of granite under high pressure, J. Geophys. Res. 73 (1968) 2225–2236.
[9] P.A. Hsieh, J.V. Tracy, C.E. Neuzil, J.D. Bredehoeft, S.E. Silliman, A transient laboratory method for deteriming the hydraulic properties of "tight" rocks-I. Theory, J. Rock. Mech. Min. Sci. & Geomech. Abstr. 18 (1981) 245–252.
[10] I. Song, J. Renner, Linear pressurization method for determining hydraulic permeability and specific storage of a rock sample, Geophys. J. Int. 164 (2006) 685–696.
[11] P.K. Mehta, P.J.M. Monteiro, Concrete, 3rd ed., McGraw-Hill, New York, 2006, pp. 467–470.
[12] Z.C. Grasley, D.A. Lange, M.D. D'Ambrosia, Drying stresses and internal relative humidity in concrete, in: J. Skalny, F. Young (Eds.), Materials Science of Concrete, vol. VII, American Ceramic Society, 2005.
[13] O. Coussy, Poromechanics, Wiley, West Sussex, England, 2004.
[14] M.A. Biot, General theory of three-dimensional consolidation, J. Appl. Phys. 12 (1941) 155–164.
[15] J.R. Rice, M.P. Cleary, Some basic stress diffusion solutions for fluid-saturated elastic porous media with compressible constituents, Rev. Geophys. Space Phys. 14 (2) (1976) 227–241.
[16] L. Cui, Y. Abousleiman, Time-dependent poromechanical responses of saturated cylinders, J. Mech. Eng. (April 2001) 391–398.
[17] V. Baroghel-Bouny, Water vapour sorption experiments on hardened cementitious materials. Part I: Essential tool for analysis of hygral behaviour and its relation to pore structure, Cem. Concr. Res. 37 (2007) 414–437.
[18] S. Mindess, J.F. Young, Concrete, Prentice-Hall, Englewood Cliffs, NJ, 1981.
[19] W. Vichit-Vadakan, G.W. Scherer, Measuring permeability of rigid materials by a beam-bending method: III. Cement paste, J. Am. Ceram. Soc. 85 (6) (2002) 1537–1544; Erratum, J. Am. Ceram. Soc. 87 (8) (2002) 1615.
[20] G.W. Scherer, Dynamic pressurization method for measuring permeability and modulus: I. Theory, Mat. Struct. 3 (2006) 1041–1057.

[21] R.C. Weast, M.J. Astle (Eds.), CRC Handbook of Chemistry and Physics, 62nd ed., CRC Press, Boca Raton, FL, 1981.
[22] Wolfram Research, Inc., 100 Trade Center Drive, Champaign, IL, 61820-7237, USA.
[23] Z.C. Grasley, G.W. Scherer, D.A. Lange, J.J. Valenza II, Dynamic Pressurization Method for Measuring Permeability and Modulus: II. Cementitious materials, Mat. Struct. 40 (7) (2007) 711–721.
[24] G.W. Scherer, Measuring permeability of rigid materials by a beam-bending method: I. Theory, J. Am. Ceram. Soc. 83 (9) (2000) 2231–2239. Erratum, J. Am. Ceram. Soc. 87 (8) (2000) 1612–1613.
[25] G.W. Scherer, Measuring permeability of rigid materials by a beam-bending method: IV. Transversely isotropic plate, J. Am. Ceram. Soc. 87 (8) (2004) 1517–1524.
[26] G.W. Scherer, Thermal expansion kinetics: method to measure permeability of cementitious materials: I, Theory, J. Am. Ceram. Soc. 83 (11) (2000) 2753–2761; Erratum, J. Am. Ceram. Soc. 87 (8) (2000) 1609–1610.
[27] G.W. Scherer, Thermal expansion kinetics: method to measure permeability of cementitious materials: III, effect of viscoelasticity, J. Am. Ceram. Soc. 87 (8) (2004) 1509–1516.
[28] J.J. Valenza, G.W. Scherer, Evidence of anomalous thermal expansion of water in cement paste, Cem. Concr. Res. 35 (2005) 57–66.
[29] F.B. Hildebrand, Advanced Calculus for Applications, Prentice-Hall, Englewood Cliffs, New Jersey, 1962.